

contact angle will be greater than zero for $T < T_{AL}$. Careful measurements of adsorption isotherms would appear to provide the simplest means of testing our predictions. Neutron scattering experiments could, in principle, provide a wealth of detail about $n(z)$.

*Work partially supported by National Science Foundation Grant No. DMR75-21866.

¹See, e.g., J. G. Dash, *Films on Solid Surfaces* (Academic, New York, 1975).

²C. Ebner, W. F. Saam, and D. Stroud, *Phys. Rev. A* **14**, 2264 (1976).

³Density profiles for bulk superfluid He⁴ in the presence of such a potential are reported by C. Ebner and W. F. Saam, in *Proceedings of the Fourteenth International Conference on Low Temperature Physics*, edited by M. Krusius and M. Vuorio (American Elsevier, New York, 1975), Vol. I, p. 447.

⁴The potential parameters are such that the hard-core diameter is the mean of the CO₂ and argon hard-core diameters while the van der Waals attraction is equal to the square root of the product of the argon and CO₂ van der Waals attractions. The argon interaction was chosen as in Ref. 2 while the CO₂ potential was taken from J. A. Hirschfelder, C. F. Curtiss, and R. B. Bird, *Molecular Theory of Gases and Liquids* (Wiley, New York, 1954), p. 1111. Finally, n_w is the number density of solid CO₂ at $T = 100$ K as reported by

O. Maass and W. H. Barnes, *Proc. Roy. Soc. London, Ser. A* **111**, 224 (1926).

⁵The trial function used is

$$n(z) = \left[\frac{\beta}{\exp[\gamma(z - \delta)] + 1} + \sum_{j=1}^5 \theta_j z^{j-1} \exp(-\epsilon z^2) + n_w \right] \times \exp\left(-\frac{\alpha z^{-9}}{T}\right),$$

where α , β , γ , δ , ϵ , and the five θ_j 's are the variational parameters. This function $\sim \exp(-\alpha z^{-9}/T)$ for small z ; it can oscillate by virtue of the power series; and, for the case of relatively thick films, $\beta + n_w$ is the density of the film, δ is approximately its thickness, and $1/\gamma$ is the width of the transition region between the liquid film and the vapor which has density n_w .

⁶The possibility of such a transition appears to be hinted by L. D. Landau and E. M. Lifshitz, *Statistical Physics* (Addison-Wesley, Reading, Mass., 1969), p. 469. This material is not contained in the 1958 edition.

⁷M. Chester, D. F. Brewer, L. C. Yang, and K. A. Elinger, *J. Phys. C* **7**, 1949 (1974) present a phenomenological local density-functional theory of adsorbed films. This theory uses the pressures at which liquefaction and solidification occur in the bulk to determine the location of the solid-liquid and liquid-gas interfaces in the film. The density profile of the adsorbate cannot be found using this formalism; interestingly, however, it predicts that a helium film adsorbed on Grafoil will have one or two solid atomic layers at its base—a result similar to what we have found for argon on CO₂.

Shubnikov-de Haas Oscillations in a Semiconductor Superlattice*

L. L. Chang,† H. Sakaki,‡ C. A. Chang, and L. Esaki
IBM Thomas J. Watson Research Center, Yorktown Heights, New York 10598
(Received 9 February 1977)

We have observed Shubnikov-de Haas oscillations associated with the quantum sub-bands created in superlattices made of periodic layers of GaAs and Ga_{1-x}Al_xAs. By controlling the periodic potential profile, a variety of sample with sub-bands of different degrees of two-dimensionality have been prepared for investigation. The observed oscillatory behaviors agree with those predicted from the Fermi surfaces calculated theoretically on the basis of the superlattice configuration and the electron concentration.

The investigation of quantum sub-bands has been one of the major objectives in the studies of a semiconductor superlattice—a periodic structure made of alternating, ultrathin layers of two semiconductors. Experiments reported to date,^{1,2} including the recent resonant Raman scattering measurements,³ have largely established the existence of such sub-bands, their energy positions, and their influence on the dynamics of electrons moving perpendicularly to the layers. In this Letter, we report the first observation of magnetoquantum oscillations (Shubnikov-de Haas

effect) in superlattices with the current flowing in the plane of the layers. The superlattice provides a unique medium where the bandwidths of the sub-bands can be controlled by selecting the barrier and well thicknesses as well as the barrier height. The observed oscillations manifest the electronic sub-band structure, which becomes increasingly two-dimensional in character as the bandwidths is narrowed.

Figure 1 illustrates three sub-band structures (A), (B), and (C), with a superlattice energy diagram shown schematically in the upper panel:

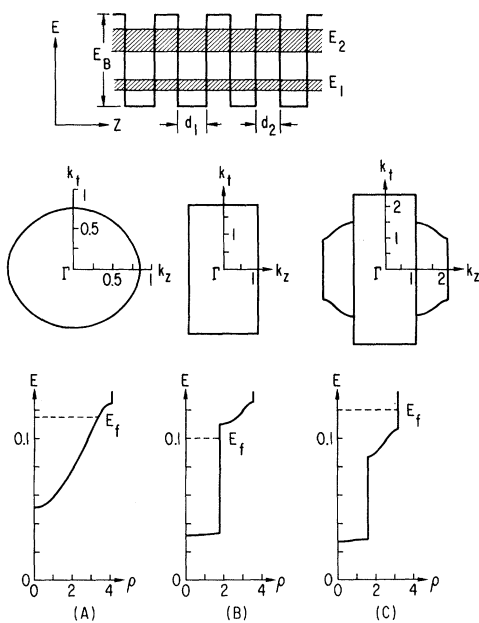


FIG. 1. A schematic superlattice energy diagram (upper panel), together with calculated Fermi surfaces in the t - z plane in \vec{k} space, and the densities of states. (t refers to the x - y plane—the plane of the layers.) Three situations are illustrated, whose configurations are described in the text. The units used are \vec{k} in π/d cm^{-1} , where $d=d_1+d_2$ is the period, ρ in $10^{19} \text{ cm}^{-3} \text{ eV}^{-1}$, and E in eV.

a periodic potential of height E_B and period d , consisting of wells of width d_1 and barriers of width d_2 , in the z direction. The energy in general is given by $E = \hbar^2 k_t^2 / 2m_t + E_z(k_z)$, where \vec{k} and m are the wave vector and the effective mass, respectively, and the subscript t refers to quantities in the x - y plane of the layers. For a three-dimensional spherical band, E_z is given by $\hbar^2 k_z^2 / 2m_z$ with $m_z = m_t$. The introduction of a superlattice potential creates a series of quantum sub-bands, the two lowest in energy being E_1 and E_2 with zone boundaries at $k_z = \pm \pi/d$ and $\pm 2\pi/d$. The energy positions and E_z - k_z relationships of the sub-bands can be calculated numerically based on the superlattice configuration by use of the Kronig-Penney model.¹ The Fermi surfaces can in turn be calculated, once the electron concentrations are known. Figure 1(a) shows the case of a relatively weak potential, for which the E_1 sub-bandwidth is rather wide, 71.1 meV, and the projection of the Fermi surface on the t - z plane deviates only slightly from a circle. An increase in the strength of the superlattice potential enhances this anisotropy, leading eventually to a discrete

bound state in E_z and a two-dimensional sub-band characterized by an energy-independent density-of states and a cylindrical Fermi surface. Figure 1(b) represents the case with an extremely narrow E_1 sub-bandwidth of 2 meV and a projected Fermi surface which is essentially rectangular. The situation shown in Fig. 1(c) can be looked upon as a composite case in that electrons occupy both a narrow ground sub-band, $E_1 = 2.3$ meV, and a relatively wide second sub-band, $E_2 = 20.2$ meV. The results drawn here are based on actual superlattice configurations of GaAs wells and $\text{Ga}_{1-x}\text{Al}_x\text{As}$ barriers, using $m_t = 0.07m_0$ and values of E_B from the conduction-band discontinuities¹: (a) $d_1 = 40 \text{ \AA}$, $d_2 = 30 \text{ \AA}$, $x = 0.16$, and $n = 1.4 \times 10^{18} \text{ cm}^{-3}$; (b) $d_1 = 90 \text{ \AA}$, $d_2 = 75 \text{ \AA}$, $x = 0.17$, and $n = 1.2 \times 10^{18} \text{ cm}^{-3}$; and (c) $d_1 = 90 \text{ \AA}$, $d_2 = 90 \text{ \AA}$, $x = 0.11$, and $n = 1.9 \times 10^{18} \text{ cm}^{-3}$. The electron mobility in all three samples is about $1200 \text{ cm}^2/\text{V sec}$. These samples were grown on semi-insulating GaAs substrates by molecular-beam epitaxy⁴ with a total superlattice thickness of about $2 \mu\text{m}$. Both the electron concentration n and the mobility were obtained from Hall measurements while the thicknesses and composition were determined from calibrated growth rates.⁴

The percentage change of the magnetoresistance, $\Delta R/R_0$, measured at 4.2°K as a function of magnetic field, \vec{H} , is shown in Fig. 2 for sample (C). Long-bar-shaped geometry, as illustrated in the inset, has been used throughout the present experiments with a typical length-to-width ratio of 30. The current flows in the x direction while \vec{H} is applied in the y - z plane with the angle φ defined with respect to the y axis. It is seen that, in the region of high angles, well-defined oscillations exist with the extremal points apparently shifting toward high fields and gradually disappearing as φ is decreased. Their evanescence at low angles reveals that there remains a different, albeit less pronounced, set of oscillations. Well-defined oscillations were also observed in samples (A) and (B) with, however, some significant distinctions: Only a single set of oscillations exists; it persists for all orientations of the magnetic field with a rather weak dependence in sample (A), whereas the characteristics in sample (B) are similar to those in sample (C) at high angles but become featureless in the low-angle region.

Under the condition of magnetic quantization for closed and nonintersecting orbits, the constant-energy surface in \vec{k} space perpendicular to the field becomes quantized according to the Onsager

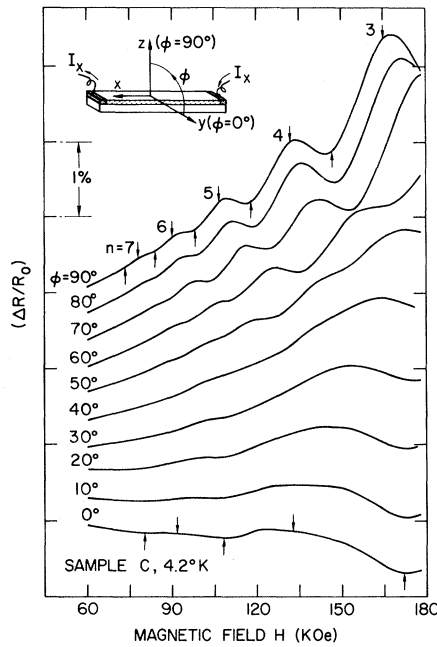


FIG. 2. Magnetoconductance vs magnetic field applied at different orientations as defined in the inset. Extrema of oscillations are indicated by arrows. Integers identify the quantum number of the magnetic energy states.

rule: $(2\pi eH/\hbar c)(n + \gamma) = A_n$, where A_n is the area of the cross section corresponding to the energy state whose quantum number is n , an integer, and γ is a phase factor lying between 0 and 1. Theoretical considerations have shown that magnetoconductance exhibits an oscillatory behavior with respect to the field.⁵ The extremal points in the resistance occur whenever $A_n = A_F$ and the period in ΔH^{-1} is given by $2\pi e/\hbar c A_F$, where A_F is the extremal cross section of the Fermi surface perpendicular to the field. Referring to Figs. 1 and 2 for the case of $\phi = 90^\circ$ at which the magnetic field is perpendicular to the superlattice plane, the quantization condition and the period of oscillation are reduced to the more commonly used expressions of $\hbar\omega_c(n + \gamma) = E_F$ and $e\hbar/cm_1 E_F$, respectively, where $\hbar\omega_c = eH/cm_1$ is the ordinary cyclotron energy. In the extreme case of a two-dimensional band, the oscillations depend only on the perpendicular component of the field,⁶ $H_z = H \sin\phi$, and the period in ΔH_z^{-1} is given by $e\hbar/cm_1 E_F$. The two-dimensional electronic system has been of great interest and extensively studied in Si and other surfaces.⁷

Values of H^{-1} at which the extremal points occur in the oscillations are plotted against n in

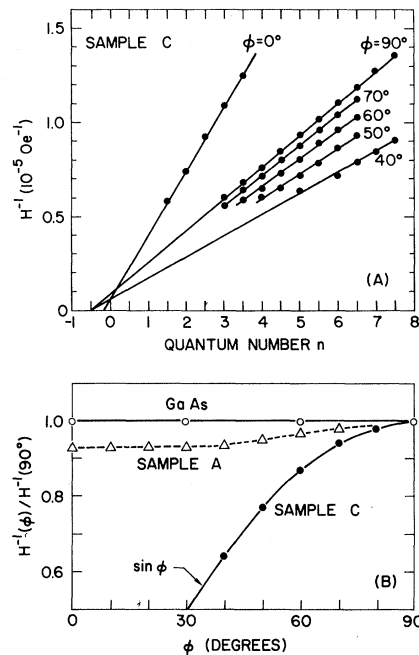


FIG. 3. Values of inverse magnetic fields at which extrema appear in the oscillations plotted vs (a) the quantum number and (b) the orientation of the field. These values are normalized in (b) to show the orientation dependence for different samples.

Fig. 3(a) for sample (C). In the region of high angles, the data fall on a set of straight lines which are consistent with a common intercept of $-\frac{1}{2}$ on the abscissa. The quantum numbers here are identified by assigning integers to maxima and half-integers to minima and by demanding that the intercept be in the range between 0 and -1 . The slope as evaluated from the line at $\phi = 90^\circ$ gives a Fermi energy of 97 meV, with use of $m_t = 0.07m_0$ as before. This value agrees remarkably well with that shown in Fig. 1(c), 96 meV, as measured from the ground sub-band E_1 , which was calculated based on the measured number of electrons filling in both of the sub-bands. It may be worthwhile to point out, in this connection, that the calculated E_F would be 75 meV for three-dimensional GaAs, and 119 meV if one considers only the ground sub-band and ignores the second sub-band. A similar degree of agreement was also observed in other samples where only the ground sub-band is involved as shown in Figs. 1(a) and 1(b): a measured value of 69 meV vs a calculated one of 63 meV in sample (A), and an identical value of 69 meV in sample (B). The phase factor, depending on both the dimensionality of the bands and the complex scattering mech-

anism, has been a subject of considerable theoretical interest.^{5,8} For noninteracting magnetic quantum states in a two-dimensional electronic system, it is expected to be one-half⁸ as observed here experimentally for the ground sub-band in sample (C). The contribution from electron spin, unlike that in Si,⁹ is negligible in GaAs.⁵

Also plotted in Fig. 3(a) are the data points obtained at $\varphi = 0^\circ$ for sample (C), although here the oscillations are less well defined as seen from Fig. 2, particularly with regard to the last maximum position. It is likely that they are associated with electrons in the second sub-band which, being somewhat three-dimensional in character, could cause oscillations even in this field orientation. These oscillations would have a large period because of the small Fermi cross section of the second sub-band. The lack of such oscillations in sample (B) is consistent with this interpretation, since the second sub-band is not expected to be occupied. The electron orbit in this case, however, becomes open at the zone boundary at $k_z = \pm 2\pi/d$ as shown in Fig. 1(c), and would have to be closed by magnetic breakdown to give rise to oscillations.¹⁰ The generally accepted condition for magnetic breakdown is approximately $(\hbar\omega_c E_F/E_g^2) \geq 1$. If we use the calculated energy gap between the second and third sub-bands, $E_g = 30$ meV, the magnetic field required would be about 100 kOe which is an overestimate because the Fermi energy is below the edge of the third sub-band. This would suggest, in any case, that magnetic breakdown may indeed be taking place in the range of magnetic fields in this investigation. To match the observed period, however, an area of the Fermi surface about twice as large as that calculated from Fig. 1(c) for the second sub-band would be needed, which would imply electrons traversing to a neighboring zone for completion of the breakdown process.

The dependence of the oscillations on the orientation of the magnetic field is plotted in Fig. 3(b) in a normalized fashion so that it applies to states of all quantum numbers. Included in the plot for comparison is the dependence obtained from a pure GaAs film, whose three-dimensional spherical energy surface results in an orientation-independent behavior as expected. In fact, essentially the same behavior has also been observed in a superlattice containing 40 Å of GaAs and 40 Å of Ga_{1-x}Al_xAs with $x = 0.05$. The weak periodic potential in this case, giving rise to a rather wide sub-band (more than 70 meV) extending beyond

the barrier height, makes the Fermi surface essentially spherical and hardly distinguishable from that of pure GaAs. The data of sample (A), which exhibit a relatively weak orientation dependence as mentioned earlier, are connected by a dotted line in the figure. Its intercept at $\varphi = 0^\circ$, as calculated from the ratio of the Fermi surface from Fig. 1(a) to the corresponding circular surface in the x - y plane, is 0.93, in excellent agreement with the experimental value as seen in Fig. 3(b). The results from both samples (B) and (C) at large angles, the latter shown in Fig. 3(b), follow strictly the theoretically expected sine relationship, indicating clearly the two-dimensional nature of the ground sub-bands.

To conclude, what we have presented in this Letter are characteristics of magnetoquantum oscillations in a few exemplary superlattices. The excellent agreement between the experimental observations and the theoretical calculations—not only in the Fermi energy or the period of oscillations but also in their dependence on the field orientation—has demonstrated and brought into focus the central feature of a semiconductor superlattice, that of control of sub-band dimensionality and anisotropy.

We are grateful to G. A. Sai-Halasz for participating in the band calculations, to A. Segmüller for x-ray measurements used in calibrating the growth rates, to F. Stern for helpful discussions, and L. S. Osterling, M. S. Christie, and C. C. Periu for their technical assistance. We also want to express our special thanks to L. G. Rubin of the Francis Bitter National Magnet Laboratory, whose cooperation has made this work possible.

*Work sponsored in part under U. S. Army Research Office Contract.

†Part of this work was performed while the authors were guest scientists at the Francis Bitter National Magnet Laboratory, which is supported at Massachusetts Institute of Technology by the National Science Foundation.

‡On leave from the Institute of Industrial Science, University of Tokyo, Tokyo, Japan.

¹See a recent review by L. Esaki and L. L. Chang, *Thin Solid Films* **36**, 285 (1976).

²R. Dingle, A. C. Gossard, and W. Wiegmann, *Phys. Rev. Lett.* **34**, 1327 (1975).

³P. Manuel, G. A. Sai-Halasz, L. L. Chang, C. A. Chang, and L. Esaki, *Phys. Rev. Lett.* **37**, 1701 (1976).

⁴L. L. Chang and R. Ludeke, in *Epitaxial Growth*, edited by J. W. Matthews (Academic, New York, 1975), p. 37.

⁵L. M. Roth and P. N. Argyres, in *Semiconductors*

and *Semimetals*, edited by R. K. Willardson and A. C. Beer (Academic, New York, 1966), Vol. 1, p. 159.

⁶F. Stern and W. E. Howard, *Phys. Rev.* **163**, 816 (1967).

⁷See, for example, *Proceedings of the International Conference on Electronic Properties of Quasi-Two-Dimensional Systems, Providence, Rhode Island, 1976*, edited by J. J. Quinn and P. J. Stiles (North-Holland,

Amsterdam, 1976) as reprinted from *Surface Science* **58**, 1976.

⁸T. Ando and Y. Uemura, *J. Phys. Soc. Jpn.* **36**, 959 (1974).

⁹F. F. Fang and P. J. Stiles, *Phys. Rev.* **174**, 823 (1968).

¹⁰M. H. Cohen and L. M. Falicov, *Phys. Rev. Lett.* **7**, 231 (1961).

Positron Self-Trapping in ⁴He

M. J. Stott* and E. Zaremba

Department of Physics, Queen's University, Kingston, Ontario, Canada K7L 3N6

(Received 7 April 1977)

Positron-annihilation experiments in helium gas have shown anomalies in annihilation rate near the gas-liquid critical point which indicate the formation of positron self-trapped states in helium droplets. We present theory which appears to confirm the existence of self-trapped states and accounts quantitatively for the positron-annihilation rate in the range of densities and temperatures over which these states are stable. The droplets have a maximum density $2.4 \times 10^{22} \text{ cm}^{-3}$ and are typically 15 to 25 Å in radius.

The positron-lifetime spectrum in helium in the vicinity of the gas-liquid critical point has been observed to possess a number of unusual features.¹ At some time ($\approx 10 \text{ nsec}$) after the introduction of positrons into the gas, the positron annihilation rate is found to increase suddenly to a value corresponding to liquid densities. A qualitative explanation of this behavior was the suggestion² that the increased rate was due to the annihilation of the positron from a localized state confined within a high-density helium cluster, the state being populated after sufficient time had elapsed for the positron to have thermalized. Subsequent measurements³⁻⁵ have confirmed the effect and have established the range of gas densities and temperatures over which the enhanced annihilation rate occurs.

In contrast to this behavior for the positron it is well known that electrons in helium⁶ and positronium in many liquefied gases⁷ may be self-trapped in bubbles. The possibility of positron self-trapping in metals has been studied theoretically⁸ but experimental evidence is inconclusive. Helium appears to be the first system for which positron self-trapping is definitely exhibited. It is, therefore, of interest to understand the nature of positron self-trapping in helium and

to determine those properties which make the self-trapped state stable. In this Letter we present a theory which can account quantitatively for most of the experimental observations on this system.

Initial attempts³ to account for the self-trapped state were based on Atkin's "snowball" model⁹ used in describing the helium density distribution around a fixed ion. This calculation, which treats the positron-helium interaction from a macroscopic point of view, fails to produce a self-trapped state since it does not fully account for the energetics of a positron in a polarizable medium. Provided that the spatial variation of the helium density is small on the scale of the range of the positron-helium interaction, the relevant quantity is the ground-state energy of a positron, $E_0(n)$, in a uniform system of mean density n . Since the net interaction is attractive, $E_0(n)$ is negative and decreases in value with increasing helium density. It is this feature, together with the easy compressibility of the gas near the critical point, which leads to the stability of the self-trapped state.

An approximate thermodynamic potential which describes the fully interacting positron-helium system is

$$\Omega[n, \psi] = \int d^3r f(n(\vec{r}))n(\vec{r}) - \mu(n_0) \int d^3r n(\vec{r}) + \int d^3r \int d^3r' K(\vec{r}, \vec{r}'; [n]) [n(\vec{r}) - n(\vec{r}')]^2 - (\hbar^2/2m) \int d^3r \psi^*(\vec{r}) \nabla^2 \psi(\vec{r}) + \int d^3r E_0(n(\vec{r})) |\psi(\vec{r})|^2. \quad (1)$$